

# Signature of a Cosmic String Wake at $z = 3$

Disrael Camargo Neves da Cunha<sup>\*1</sup>

<sup>1</sup>*Department of Physics, McGill University, Montreal, QC, H3A 2T8, Canada*

(Dated: March 5, 2022)

In this paper, we describe the results of N-body simulation runs which include a cosmic string wake of tension  $G\mu = 10^{-7}$  on top of the usual  $\Lambda$ CDM fluctuations. To obtain a higher resolution of the wake in the simulations compared to previous work, we insert the effects of the string wake at a lower redshift and perform the simulations in a smaller box. A curvelet analysis of the wake and no wake maps is applied, indicating that the presence of a wake can be extracted at four sigma confidence level from maps of the two-dimensional dark matter projection down to a redshift of  $z = 3$ .

## Contents

<b>I. Introduction</b>	1
<b>II. Review of Cosmic string wakes in the non-linear regime</b>	2
<b>III. Simulations</b>	3
<b>IV. Analysis</b>	3
A. A curvelet filtering of the two-dimensional projections	5
B. Wake signal extraction with wake orientation prior	6
C. Wake signal extraction without wake orientation prior	7
<b>V. Conclusion</b>	8
<b>Acknowledgement</b>	8
<b>References</b>	8

## I. INTRODUCTION

Cosmic strings are linear topological defects in Quantum Field Theory which exist as solutions in some models that go beyond the Standard Model of Particle Physics [1]. A cosmic string consists of a one-dimensional region of trapped energy, having significant gravitational effects for cosmology. If a model of nature admits cosmic string solutions, strings will necessarily form during the early universe [2]. For example, in some models, they form after the end of inflation, and in others, they form during a phase transition in the early radiation phase of Standard Big Bang Cosmology. After the cosmic strings form, they will persist as a scaling network. This means that the network of cosmic strings will have the same properties at all times if we scale the length observables to the Hubble radius [2]. The network will consist of a few long strings

moving near the speed of light and also of loops of different sizes, and it will source sub-dominant fluctuations at all times. The gravitational effects of a cosmic string are characterized by only one number  $\mu$ , its tension, which does not affect the scaling solution properties of the cosmic string network. The tension can also be seen as the energy per unit of length of the cosmic string, and it is related to the energy scale  $\eta$  at which the strings form by the following equation:

$$G\mu \simeq (\eta/m_{pl})^2 \quad (1)$$

where  $G$  is Newton's constant and  $m_{pl}$  is the Planck mass. The presence of cosmic strings does not produce acoustic oscillation features on the Cosmic Microwave Background (CMB) angular power spectrum. This fact contributes to the current upper bound <sup>1</sup> on the cosmic string tension [3]:

$$G\mu \approx 1.5 \times 10^{-7} \quad (2)$$

A good study on the observational aspects of cosmic strings has two possible outputs [4]. One possibility is observing a cosmic string, which would be a significant achievement on probing particle physics models beyond the Standard Model of Particle Physics. The other option is not to observe cosmic strings, which will lower the bound on the cosmic string tension, thus ruling out classes of particle physics models. Besides this, cosmic strings could produce interesting results for cosmology such as explaining the origin of Fast Radio Bursts [5], primordial magnetic fields [6], and the origin of super-massive black holes [7].

<sup>1</sup> Note that there are stronger limits on the string tension which comes from limits on the stochastic background of gravitational waves on length scales which the pulsar timing arrays are sensitive to (see e. g. [19]). These bounds come from gravitational radiation from string loops, and assume a scaling distribution of string loops where the total energy in strings is dominated by the loops [20]. However, field theory cosmic string simulations [21] do not yield a significant distribution of string loops. Thus, bounds on the cosmic string tension from gravitational radiation from string loops are less robust than the ones coming from the long strings.

\*camargod@hep.physics.mcgill.ca

This work will concentrate on the Large Scale Structure (LSS) as a complementary (in addition to the CMB) arena for probing cosmic string. The primary motivation is that LSS data contains three-dimensional information, which includes many more modes than the two-dimensional maps from the CMB. The disadvantage of LSS is that the effects of non-linearities are essential, so theoretical predictions are harder to be obtained.

In a recent paper [8] (see also [9]) we began a study of the dark matter distribution induced by string wakes [10] inserted at  $z = 31$ , using a simulation box of lateral size  $L = 64Mpc/h$  and  $np = 512$  particles per dimension. We found that the string signals for a wake with a string tension of  $G\mu = 10^{-7}$  can be identified down to a redshift of  $z \geq 10$ . A possible cause for not being able to identify the wake at lower redshifts comes from the fact that the wake thickness was about one order of magnitude smaller than the resolution length of the simulation grid at the time of wake insertion. The fact that the wake survives down to redshift  $z = 10$  supports the idea that the wake global signal remains present despite losing its local signal [13]. In the current work, we take a complementary approach, and we use a box with a small lateral size (of  $L = 4Mpc/h$ ) and a higher number of particles ( $np = 1024$  particles per dimension), so the wake becomes well-resolved. The downside of this approach is that we lose part of the global wake signal and the advantage is that the effect of the wake lasts for more time.

A cosmic string wake is a planar overdense region that forms behind a long string as it passes by the matter distribution [10]. This effect is a consequence of the fact that a space perpendicular to the long string will have a missing angle given by  $\alpha = 8\pi G\mu$  [1], causing two test dark matter particles initially at rest to receive a velocity kick towards behind the string as soon as it passes by between the two. The expression for the velocity perturbation is the following:

$$\delta v = 4\pi\gamma_s v_s G\mu \quad (3)$$

where  $v_s$  is the transverse velocity of the string and  $\gamma_s$  is the associated Lorentz factor. The velocity kick makes the particles meet behind the string, forming a wedge-like structure with two times the average matter density. This is the wake. The initial geometry of the wake after formation at  $t = t_{wf}$  will be a box of volume  $V$ , consisting of two large planar dimensions of the order of the Hubble radius  $\approx t_f$  and one smaller thickness with a length of the order of the Hubble radius multiplied by the deficit angle:

$$V \approx t_f \times t_f v_s \gamma_s \times 4\pi G\mu t_f v_s \gamma_s \quad (4)$$

At early times it is possible to obtain an analytical understanding of the wake evolution thanks to the fact that the matter fluctuation outside the wake was in the linear regime. The Zeldovich approximation [11] gives the evolution of the comoving wake thickness  $\psi_3$  as a

function of redshift  $z$  [12] :

$$\psi_3 = \frac{24\pi}{5} G\mu v_s \gamma_s t_0 \frac{\sqrt{1+z_{eq}}}{(1+z)} \quad (5)$$

where  $t_0$  is the present time and  $z_{eq}$  is the redshift of matter and radiation equality. Note that the wake produces a nonlinear density fluctuation at arbitrarily early times. Since structures start to grow only after the time of equal matter and radiation, we choose this time as the time for wake formation (so we will consider  $t_f = t_{eq}$ ). We use the value  $z_{eq} = 1000$ . As the thickness grows as in linear theory, the planar dimension increases just with the Hubble flow, and are fixed in comoving coordinates. For the formation time we are considering, the planar dimension of the wake is about  $\approx 100Mpc$ . If the analytical thickness evolution remains valid up to today, we would have wakes with the thickness of  $\approx 0.1Mpc$  at present (for  $G\mu = 1 \times 10^{-7}$ ).

Once the  $\Lambda$ CDM perturbations enter the nonlinear regime (at about the time of re-ionization), the local mass distribution in the wake becomes highly nonlinear, the  $\Lambda$ CDM fluctuations will disrupt the wake [13], and the subsequent dynamics has to be studied numerically. In this paper, we simulate cosmic string wakes using an N-body code called CUBEP3M [14] and apply a statistic that extracts the wake signal.

The paper is organized as follow: section II contains a discussion on the previous works regarding wake evolution in the nonlinear regime; Section III describes the simulations performed in the present work, and the analysis of the data described in section III is performed in section IV; Finally, in section V we summarize the essential results obtained and indicate experimental prospects and possible paths for an extension of the analysis.

## II. REVIEW OF COSMIC STRING WAKES IN THE NON-LINEAR REGIME

The wake produces a planar non-linear density perturbation at arbitrarily early times, so early on the wake is unambiguously distinguishable from  $\Lambda$ CDM fluctuations. Once the  $\Lambda$ CDM fluctuations start to dominate, nearby halos begin to accrete material from the wake, causing wake fragmentation. An analytical study regarding the wake disruption by  $\Lambda$ CDM fluctuations was presented in [13], where two criteria for wake disruption were introduced. The first one concerns local stability, which was studied by considering a cubic box with the dimension of the wake thickness and computing the standard deviation of the density contrast in this region from  $\Lambda$ CDM fluctuations. The second criterion takes the global extension of the wake region into account, by computing the standard deviation of the density contrast from  $\Lambda$ CDM inside a box with dimension  $V$  (see (4)) given by the whole wake. Both conditions were computed, and the main result indicates that although a  $G\mu = 10^{-7}$  wake could be locally disrupted at  $z \approx 8$

it could in principle be distinguished from  $\Lambda$ CDM fluctuations at all times using the global information of the wake.

A method used to extract the wake signal from the dark matter distribution was presented in [8] and can be summarized as follows: for any direction of the sphere, we consider an associated projection axis passing through the origin of the box. We then consider slices of the simulation box perpendicular to that axis at each point  $x$  of this axis with thickness given by the grid size of the simulation, and we compute the mass density  $\delta(x)$  of dark matter particles in that slice as a function of  $x$ . A one-dimensional filter wavelet analysis is then performed on the mass density  $\delta(x)$ , giving a filtered version of it, called  $f\delta$ . We then compute the maximum value  $S$  of  $f\delta(x)$  for each direction (pair of spherical angles) in the simulation box.  $S$  is a map on the surface of the sphere (which represent the spherical angles), and  $\hat{S}$  is its maximum value. The signal to noise ratio for the spherical peak ( $\max(S)$ ) divided by standard deviation ( $\max(S)/\text{std}(S)$ ) distribution for ten simulations without wake and three simulations with a  $G\mu = 10^{-7}$  wake was found to be  $\bar{\mathcal{R}} = 8.1$  at redshift  $z = 10$  and insignificant at lower  $z$ .

The setup of the N-body simulation is the following. We used an N-body simulation program called CUBEP<sup>3</sup>M, a public high performance cosmological N-body code based on a two-level mesh gravity solver augmented with sub-grid particle-particle interactions [14]. This code generates and evolves initial conditions (which are realizations of  $\Lambda$ CDM fluctuations) containing positions and velocities of particles inside a cubic box. There is an option to save the phase space of the distribution at any redshift and rerun the code from this checkpoint. We use this feature for wake insertion, by modifying the saved phase space distribution at time  $t_i$  by including effects of a wake. The modification consists in displacing and giving a velocity kick to particles towards the wake plane. The absolute value of the displacement  $\psi(t_i)$  and velocity perturbation  $\dot{\psi}(t_i)$  in comoving units can be computed using the following equations (see [12] for details)

$$\psi(t_i) = \frac{3}{5}4\pi G\mu v_s \gamma_s t_{eq} z(t_{eq}) \frac{z(t_{eq})}{z(t_i)}. \quad (6)$$

and

$$\dot{\psi}(t_i) = \frac{2}{5}4\pi G\mu v_s \gamma_s t_{eq} z(t_{eq}) \frac{z(t_{eq})}{z(t_i)} \frac{1}{t_i}. \quad (7)$$

Once the wake insertion is made, the new modified distribution is further evolved by the N-body code.

The primary goal of this paper is to find a statistic which can extract the wake presence without using information about the simulation without a wake. In the next section, we will describe the simulations in more detail.

### III. SIMULATIONS

We performed six N-body simulations without wakes with the following cosmological parameters:  $\Omega_\Lambda = 0.7095$ ,  $\Omega_b = 0.0445$ ,  $\Omega_{\text{CDM}} = 0.246$ ,  $n_t = 1$ ,  $n_s = 0.96$ ,  $\sigma_8 = 0.8628$ ,  $h = 0.70$ ,  $T_{\text{cmb}}(t_0) = 2.7255$ . Those simulations consists of  $np = 1024$  particles per dimension, a lateral size of  $L = 4Mpc/h$ , and initial conditions generated at  $z = 31$ , with checkpoints at  $z = 15$ ,  $z = 10$ ,  $z = 7$ ,  $z = 5$  and  $z = 3$ . The wake is inserted at the  $z = 10$  checkpoint. All simulations used 512 cores divided into 64 MPI tasks and were run in the Graham Cluster of Calcul Quebec, part of the Compute Canada consortium.

As pointed out in [13], if we displace all particles towards a central plane, this creates a nonphysical void on the parallel planes at the boundary of the simulation box. Here we circumvent this problem by using a suppression of the velocity and displacement perturbations that starts halfway between the wake and the boundary and linearly decreases to zero at the boundary. This procedure avoids the creation of a planar void at the boundary since the particles are not displaced there.

Figure 1 shows the average displacement induced by the wake on each particle and compares it with the analytical prediction. As in the previous work, the numerical simulation results for the wake-induced displacement are about a factor of two higher than the analytical prediction. We conjectured that this could be due to the non-physical void, but here it is evident that this was not the case since there is no void in our new simulations. This fact indicates that the analytical prediction is incomplete and we should trust more in the numerical simulations. Another reason is that we are in the non-linear regime, where the assumptions of the analytical predictions are not valid. Also, the analytical prediction assumes a late time matter dominated cosmology, whereas the numerical work is done in the context of a  $\Lambda$ CDM background. The analytical prediction should be modified for the cosmological constant dominated period. We plan to do that in the future.

A similar analysis was done for the induced velocity perturbation. As figure 2 shows, the difference between the numerical and analytical velocity perturbations is not significant.

### IV. ANALYSIS

The wake presence is not clear if we compare the visualization of a two-dimensional projection for a pure  $\Lambda$ CDM simulation with a  $\Lambda$ CDM plus wake simulation. Figure 3 illustrates this at  $z = 3$ . Both figures show the density contrast of logarithm of two-dimensional projections of the dark matter distribution (in simulation units). The upper figure contains just  $\Lambda$ CDM fluctuations, and the bottom figure contains the same  $\Lambda$ CDM fluctuations plus a  $G\mu = 10^{-7}$  wake. A trained eye could

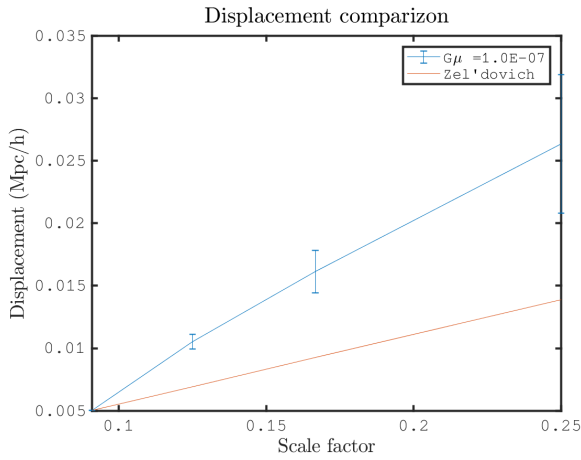


FIG. 1: Average displacement induced by the wake (in blue), compared with the analytical prediction (in red).

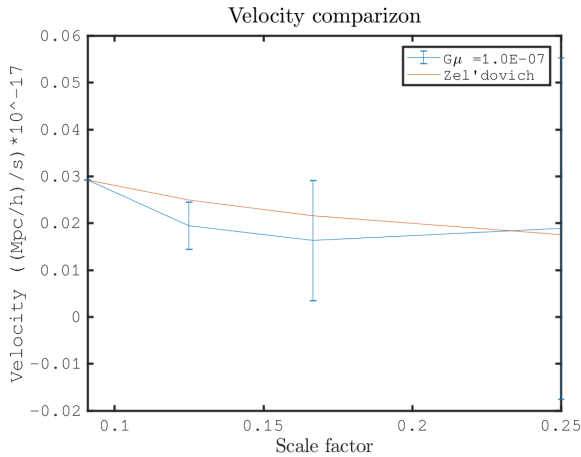


FIG. 2: Average velocity perturbation induced by the wake (in blue), compared with the analytical prediction (in red).

perceive that a wake is located at the plane  $Z \approx 2Mpc/h$  which under projection appears as a vertical line at the middle of the panel (since we are projecting onto a plane perpendicular to the wake plane). It was not possible to find a good statistics that extracts the wake signal for such projections.

This occurs because the Gaussian fluctuations displace the particles on the wake and these particles no longer form a straight plane. However, the wake can be better recovered if we project not the entire  $x$  direction, but several slices of it. It was found that if we slice the  $x$  direction in 32 different parts and perform a two-dimensional projection on each slice, the wake can be better visualized. Figure 4 shows the slice number 31 associated with the same simulations of figure 3. The wake presence is more explicit in this case and corresponds to a clear vertical line at the middle of the panel on the bottom figure of 4.

Unfortunately, this does not mean that wake detec-

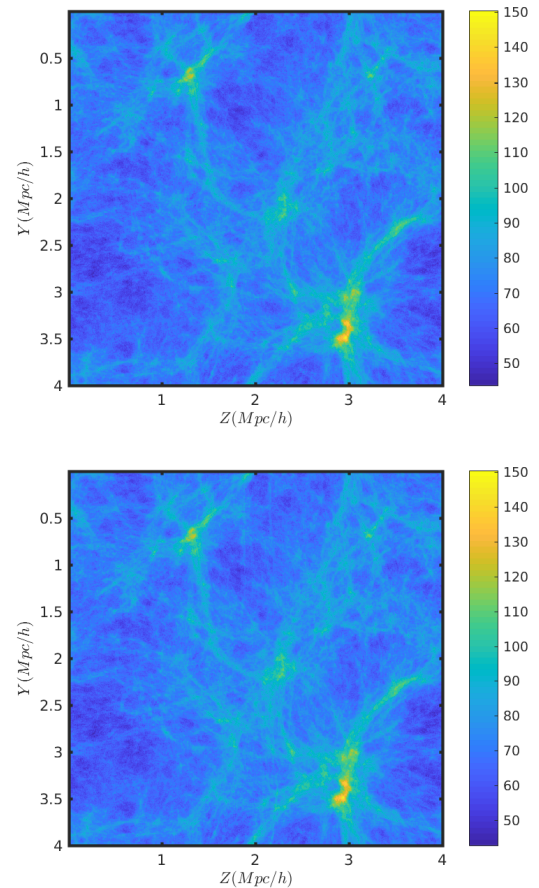


FIG. 3: Logarithm of the mass of a two-dimensional projection of simulation particles for lateral size  $L = 4Mpc/h$  and redshift  $z = 3$ . The upper plot shows the simulation without the wake, and the plot on the bottom shows the simulation with a  $G\mu = 10^{-7}$  wake at the central position of the  $z$  axis.

tion is granted since the wake presence should be obtained quantitatively and without previous knowledge of the simulation without a wake.

In the next subsection, we will show the result of a statistic that analyses a set of two-dimensional projections of the dark matter particles. We ask the question if it is possible to differentiate the images of the two-dimensional projections perpendicular to the wake from any other projection without the wake.<sup>2</sup>

A sky map with a specific redshift layer can be further subdivided into several square images (using small angle approximation), and in a universe with a cosmic string network, there is a small non-zero probability that one

<sup>2</sup> One motivation for this approach is that some experiments, like SKA [15] have a poor redshift resolution compared with the angular resolution, so the data set can be better viewed as layers of two-dimensional intensity maps with each layer corresponding to a redshift range.

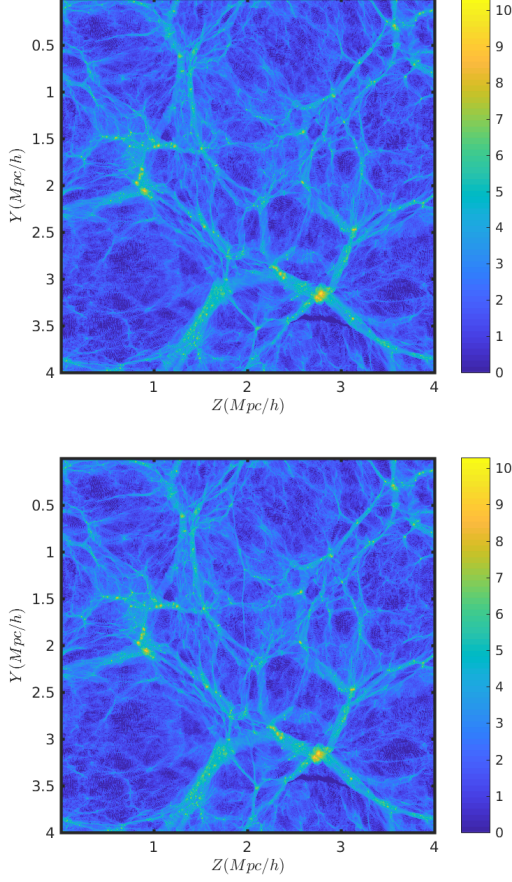


FIG. 4: Logarithm of the mass of a two-dimensional projection of a slice of the simulation box with lateral size  $L = 4Mpc/h$  and redshift  $z = 3$ . The upper plot shows the slice without the wake, and the plot on the bottom shows the slice with a  $G\mu = 10^{-7}$  wake at the central position of the  $z$  axis.

of those images has a wake perpendicular to it. We will see that this small fraction is still sufficient to pinpoint a universe with  $G\mu = 10^{-7}$  cosmic strings at redshift down to  $z = 3$ .

#### A. A curvelet filtering of the two-dimensional projections

Here we describe the pipeline for the statistics that we use for wake detection. All computations were performed using Matlab, together with the curvelet package CURVELAB [16]. We will also use ridgelet transformation [18], which detects straight lines (ridges) which cross an entire image. Similarly, the curvelet base functions are line segments, which can be seen as a local version of the ridges.

The first of the filtering procedure step is, for each cubic simulation box, to slice it into 32 different tiles (where the slice is perpendicular to the  $x$  direction, while

the wake is parallel) and to obtain a two-dimensional map of it by projecting the associated slice onto the  $y-z$  plane.

For each two-dimensional dark matter map particle number (which is proportional to the dark matter mass)  $pn$  (viewed as a two-dimensional array with the projected number of particles as each one of its elements) we perform the following steps:

1-) Compute the logarithm of the dark matter mass  $pn_{log} = \log(1 + pn)$ . The number one is added for the result to be strictly positive.

2-) Compute the curvelet-filtered transformation  $curv(s, w, i, j) = C(pn_{log})$ , where  $s$  corresponds to the scale of the ridge,  $w$  to the angle,  $i$  and  $j$  to the positions. All the curvelet coefficients with scales higher than the expected wake thickness were set to zero.

3-) A wake ridge corresponds to coefficients that are much higher than the others if we fix the position, scale and allow the angles to vary. Therefore we would like to highlight the maximum of the function  $f_{s,i,j}(w) = curv(s, w, i, j)$  in the angle variable  $w$ . We implement that for each  $(s, i, j)$  by multiplying the function  $g(w) = f_{s,i,j}(w)$  by its own density contrast  $\tilde{g}(w) = (g(w) - \bar{g})/\bar{g}$ , where  $\bar{g} = mean(g(w))$ . The resulting new wavelet coefficient becomes  $\tilde{f}_{s,i,j}(w) = f_{s,i,j}(w) \times \tilde{g}(w)$ .

4-) After the previous filter, the inverse curvelet transformation is taken and  $dm_{2d} = curv^{-1}(\tilde{f}_{s,i,j}(w))$ .

Once the 32 filtered images are computed, we combine them together again in a three-dimensional map  $dm_{3d}$ , where one of the dimension corresponds to the direction of slicing (and go from one to 32) and the remaining two dimensions are the labels for the filtered image pixels. The image of each slice corresponds to the filtered image obtained in the steps above for each one of the slices.

5-) Compute a 3d curvelet decomposition  $curv3d = C(dm_{3d})$ , and set the negative coefficients to zero. The motivation for this threshold is to consider just planar overdensity detection in the image, since the negative curvelet coefficients represent planar underdensities (or planar voids, which are not important for us). After that, we do the inverse curvelet transformation. This procedure will also highlight pixels with high density that are next to each other. By doing the inverse curvelet transformation, we obtain 32 filtered slices  $dmFilt(i, j, k) = C^{-1}(curv3d)$  from the original 32 slices, where  $i$  and  $j$  range from 1 to 1024 and  $k$  range from 1 to 32.

Steps 3 and 5 are crucial since they highlight line segment discontinuities (as produced by the wake). To see this, consider figure 5 which shows the result of the fifth step for the maps of figure 4. The wake presence is clear now, with a large line segment on the bottom panel indicating the wake position.

6-) Perform a ridgelet transformation [18] on each slice  $rad_k(l, a) = R(dmFilt_k(i, j))$ , where  $k$  indicates the slice,  $l$  the position of the ridge,  $a$  its angle and  $dmFilt_k(i, j) = dmFilt(i, j, k)$  its image before the ridgelet transformation. A ridgelet transformation is suitable for detection such as the ones produced by the wake.



7-) The wake statistical signal indicator  $s(k) = pk(k)/std(k)$  of the slice  $k$  is the peak  $pk(k) = \max(rad_k(l, a))$  divided the standard deviation  $std(rad_k(l, a))$  of the Radon transformation, where  $\max(rad_k(l, a))$  denotes the maximum value of the two dimensional array  $rad_k(l, a)$  (with respect to  $(l, a)$ ) and  $std(rad_k(l, a))$  denotes the standard deviation of the same array  $rad_k(l, a)$  (also with respect to  $(l, a)$ ). A high peak means that there is a line in the two-dimensional map with high contrast, such as the one produced by the wake.

8-) Finally, take the sum of  $s(k)$  as the wake indicator statistical signal of the  $(4Mpc/h)^3$  volume. The wake presence will increase each one of the  $s(k)$  systematically, so that is why we take their sum as the wake signal  $S$ :

$$S = \sum_k s(k) \quad (8)$$

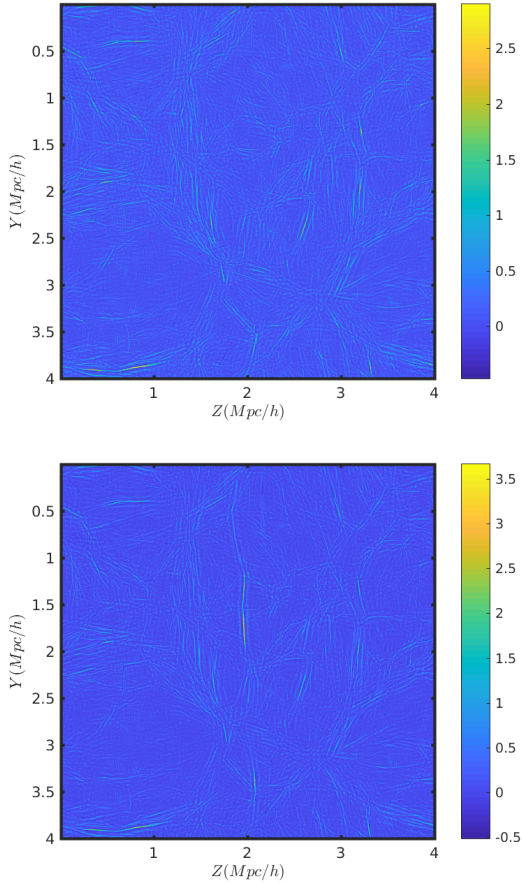


FIG. 5: Filtered version of the logarithm of the mass of a two-dimensional projection of a slice of the simulation box with lateral size  $L = 4Mpc/h$  and redshift  $z = 3$ . The upper plot shows the slice without the wake, and the plot on the bottom shows the slice with a  $G\mu = 10^{-7}$  wake at the center.

The analysis above is applied in two different situations: in the first one, the orientation of the wake is used

as prior information, and in the second situation, this information is not used beforehand. Each case will be described in the next two subsections.

### B. Wake signal extraction with wake orientation prior

We have inserted the wake at the plane  $Z = 2Mpc/h$ . Therefore, by choosing the axis  $x$  as the projection axis for our analysis, we will be automatically selecting an axis perpendicular to the wake plane and therefore will have an optimal statistical analysis.

For each simulation and orientation aligned with the wake, we chose the wake indicator  $S$  from 8. The result of the distribution of the signal  $S$  for each one of the ten simulations (with and without wakes) is shown in figure 6.

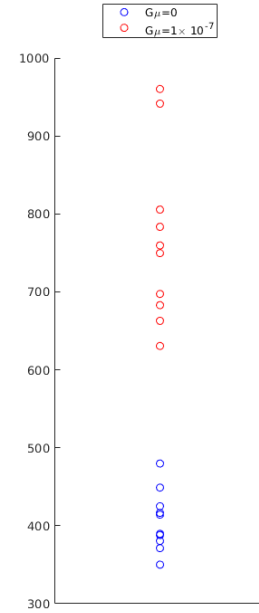


FIG. 6: Distribution of the wake indicator  $S$  for the wake simulations (in red), and with pure  $\Lambda CDM$  (in blue).

This statistic has a confidence level of  $\bar{R} = 9.9$ , where  $\bar{R} = \text{mean}(R)$  is the mean of the signal to noise ratio for the wake simulation, defined as

$$R = \frac{S - \bar{S}_{nw}}{std(S_{nw})}$$

where  $S$  is computed for a given simulation with a wake,  $\bar{S}_{nw}$  is the mean  $S$  of all simulations without wakes and  $std(S_{nw})$  is the standard deviation of all  $S$  from simulations without a wake.  $\bar{R}$  is the mean of  $R$  for all simulations with wakes.

### C. Wake signal extraction without wake orientation prior

In this subsection, we consider various orientations for the two-dimensional projections, without introducing the wake orientation information beforehand. For choosing different angular orientations, we consider a Healpix set of spherical angles [22], which give equally-spaced adjacent spherical angles. In addition to considering different orientations, we also take advantage of the periodic boundary condition and perform random displacements and rotations on the two-dimensional figures, so the wake line does not lie on the  $z = 2Mpc/h$  plane anymore. By choosing the parameter  $N_{side} = 8$  for the Healpix scheme, we can survey  $N_{angles} = 384$  different projecting angles for each simulation (we are considering just non-antipodal angles since they produce equivalent two-dimensional projections). Figure 7 shows an example for one of the simulations of a sphere in which each point is a pair of spherical angles, and the color specifies the value of the wake indicator  $S$  for that orientation.

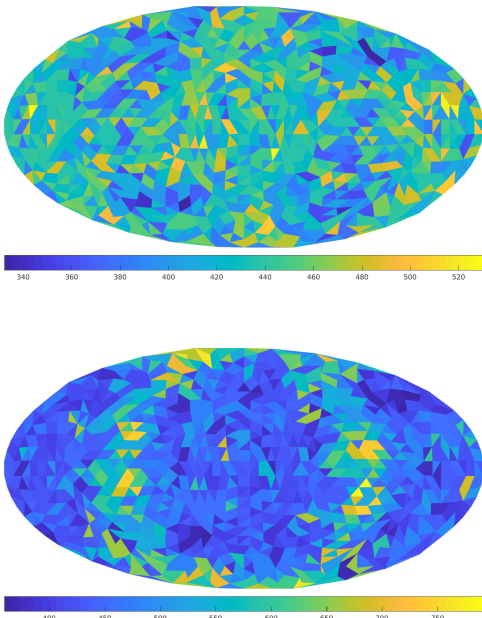


FIG. 7: Wake indicator  $S$  values for different orientations for a simulation box with lateral size  $L = 4Mpc/h$  and redshift  $z = 3$ . The upper plot shows the spherical map without the wake, and the plot on the bottom shows the spherical map with a  $G\mu = 10^{-7}$  wake.

If we consider the wake indicator  $S$  value for all angles of the ten samples, we can construct the histogram of figure 8, which shows the histograms for both the wake case and also for the no wake case.

There are 10 outliers with  $S > 532$  for the histogram without wakes and 833 outliers for the histograms with wakes. We choose  $S_t = 532$  as a threshold that indicates

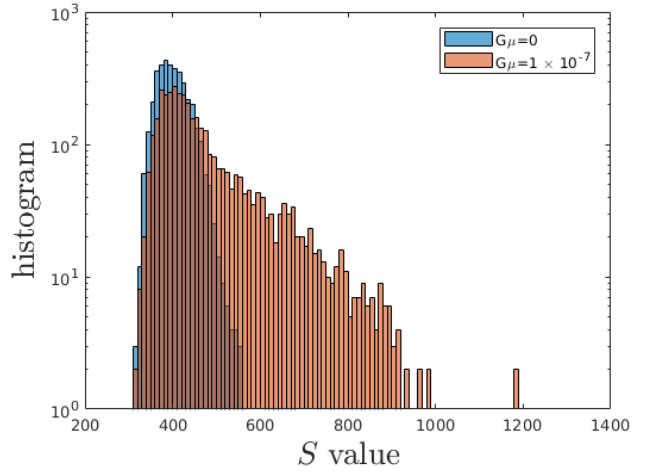


FIG. 8: Histogram in logarithmic scale of the  $S$  values for all 384 angles and ten simulation boxes with lateral size  $L = 4Mpc/h$  and redshift  $z = 3$ . The red histogram correspond to the simulations without wakes, and the blue histogram correspond to  $G\mu = 10^{-7}$  wakes.

the wake presence. In principle, we could have chosen a higher threshold, such as  $S = 590$ , where there is just one outlier for the histogram without wake and we would obtain better results (because the probability of finding such an outlier would be much smaller). But we want to construct our statistics based not in only one point, which could lead to a non-robust result. Therefore if in a pure  $\Lambda$ CDM universe a random set of 32 dark matter maps of  $(4Mpc/h)^2$  with resolution of  $1024^2$  at redshift  $z = 3$  is taken in the sky, the probability of it to have  $S > 532$  is  $p_{nw} \approx 10/3840 = 0.0026$ . We would naively expect that the probability of finding a similar  $S > 532$  dark matter maps for a universe with wakes would be  $\approx 833/3840 = 0.2169$ , but that is not true, since not every map of this kind will intercept a wake. With the simplest (and most conservative) assumption that in a  $\Lambda$ CDM plus cosmic string universe there is just one long string per Hubble volume, we would expect that only a fraction of about  $1/24 = 4Mpc/95Mpc$  of the boxes ( $95Mpc$  corresponds to the comoving Hubble radius at wake formation) would contain a wake, so we have to multiply the previous probability estimation by this factor. Therefore the expected probability of finding a similar  $S > 532$  dark matter map would be  $p_w \approx 0.2169 * (1/24) = 0.0090$ , which is 3.4 higher than in the no wake case.

We will assume that we can cover one-quarter of all angles in the entire dark matter sky, so we have about  $N = 10^4$  dark matter maps similar to the ones we are, and for each one of them, we would find one wake indicator  $S$  value. Multiplying this number  $N$  by the probability of finding  $S > 532$  outliers we expect to obtain  $N_{nw} = 26$  outliers in a universe without wakes and  $N_w = 90$  outliers in a universe with cosmic string wakes.

With this result now we can know what is the probability of discarding the null hypothesis that our universe is pure  $\Lambda$ CDM in favor of an alternative hypothesis that our universe contains a network of  $G\mu = 10^{-7}$  cosmic strings. The probability of a universe with wakes to have more than 45 (this is half the expected one, chosen to be sure the probability is very close to one) outliers from the  $N$  quantities discussed above is very close to one (by one part in  $10^7$ ). On the other hand, the probability of having more than 45 outliers in a pure  $\Lambda$ CDM universe is  $4.5594 \times 10^{-4}$ , which is a p-value equivalent to 4 sigmas of confidence level.

We showed above that it is possible to identify the presence of cosmic string wakes of  $G\mu = 10^{-7}$  at  $z = 3$  with confidence level of four sigma if a set of three-dimensional dark matter maps covering one-quarter of the sky is given. Each map should consist of 32 consecutive slices (with respect of the field of view, and having  $4Mpc/h$  of depth) of  $(4Mpc/h)^2$  squares with 1024 pixels per dimension. We argued that with the most simplistic assumptions of one wake per Hubble volume, there would be 90 outliers indicating the wake presence, whereas there will be 26 outliers in the case of a universe without cosmic string wakes.

## V. CONCLUSION

With this work, we can affirm that a sky map of the dark matter distribution can be used to constrain the existence of cosmic strings with high statistical significance.

It is worth mentioning that the values used to construct this argument are conservative ones, and increasing then (the number of maps in the sky ( $N$ ), the wake indicator threshold  $S_t = 532$ , the number of outliers 45 and the number of long cosmic strings per Hubble volume (here taken as one)) will give better results than quoted in this paper.

We are investigating whether neural networks could improve the wake detection. The hope is that they will be able to distinguish maps with and without wakes at redshifts below  $z = 3$  and lower string tension parameter.

The experimental prospects to find the wake signal will be analyzed in future works, where resolution (angular and redshift) is essential together with intensity sensitivity. Finally, it remains to be seen if the dark matter tracers, such as halos and galaxies will maintain the wake signal. All of those aspects are under current investigation.

## Acknowledgement

The author is grateful to Dr. Robert Brandenberger and Dr. Adam Amara for useful discussions and feedback. He also wishes to acknowledge CAPES (Science Without Borders) for a student fellowship. This research was enabled in part by support provided by Calcul Quebec (<http://www.calculquebec.ca/en/>) and Compute Canada ([www.computecanada.ca](http://www.computecanada.ca)). An NSERC Discovery Grant has also supported the research at McGill.

- 
- [1] A. Vilenkin and E.P.S. Shellard, *Cosmic Strings and other Topological Defects* (Cambridge Univ. Press, Cambridge, 1994);  
M. B. Hindmarsh and T. W. B. Kibble, "Cosmic strings", Rept. Prog. Phys. **58**, 477 (1995) [arXiv:hep-ph/9411342];  
R. H. Brandenberger, "Topological defects and structure formation", Int. J. Mod. Phys. A **9**, 2117 (1994) [arXiv:astro-ph/9310041].
  - [2] T. W. B. Kibble, "Phase Transitions In The Early Universe", Acta Phys. Polon. B **13**, 723 (1982);  
T. W. B. Kibble, "Some Implications Of A Cosmological Phase Transition", Phys. Rept. **67**, 183 (1980).
  - [3] C. Dvorkin, M. Wyman and W. Hu, Phys. Rev. D **84**, 123519 (2011) doi:10.1103/PhysRevD.84.123519 [arXiv:1109.4947 [astro-ph.CO]].
  - [4] R. H. Brandenberger, "Probing Particle Physics from Top Down with Cosmic Strings", Universe **1**, no. 4, 6 (2013) [arXiv:1401.4619 [astro-ph.CO]].
  - [5] R. Brandenberger, B. Cyr and A. V. Iyer, arXiv:1707.02397 [astro-ph.CO].
  - [6] R. Brandenberger, Y. F. Cai, W. Xue and X. m. Zhang, arXiv:0901.3474 [hep-ph].
  - [7] S. F. Bramberger, R. H. Brandenberger, P. Jreidini and J. Quintin, JCAP **1506**, no. 06, 007 (2015) doi:10.1088/1475-7516/2015/06/007 [arXiv:1503.02317 [astro-ph.CO]].
  - [8] D. Cunha, J. Harnois-Deraps, R. Brandenberger, A. Amara and A. Refregier, "Dark Matter Distribution Induced by a Cosmic String Wake in the Nonlinear Regime," arXiv:1804.00083 [astro-ph.CO].
  - [9] S. Laliberte, R. Brandenberger and D. C. N. da Cunha, "Cosmic String Wake Detection using 3D Ridgelet Transformations," arXiv:1807.09820 [astro-ph.CO].
  - [10] J. Silk and A. Vilenkin, "Cosmic Strings And Galaxy Formation", Phys. Rev. Lett. **53**, 1700 (1984);  
M. J. Rees, "Baryon concentrations in string wakes at  $z \gtrsim 200$ : implications for galaxy formation and large-scale structure", Mon. Not. Roy. Astron. Soc. **222**, 27 (1986);  
T. Vachaspati, "Cosmic Strings and the Large-Scale Structure of the Universe", Phys. Rev. Lett. **57**, 1655 (1986);  
A. Stebbins, S. Veeraraghavan, R. H. Brandenberger, J. Silk and N. Turok, "Cosmic String Wakes", Astrophys. J. **322**, 1 (1987).
  - [11] Y. .B. Zeldovich, "Gravitational instability: An Approximate theory for large density perturbations," Astron. Astrophys. **5**, 84 (1970).
  - [12] R. H. Brandenberger, L. Perivolaropoulos and A. Steb-



- bins, “Cosmic Strings, Hot Dark Matter And The Large Scale Structure Of The Universe,” *Int. J. Mod. Phys. A* **5**, 1633 (1990);
- L. Perivolaropoulos, R. H. Brandenberger and A. Stebbins, “Dissipationless Clustering Of Neutrinos In Cosmic String Induced Wakes,” *Phys. Rev. D* **41**, 1764 (1990).
- [13] R. H. Brandenberger, O. F. Hernández and D. C. N. da Cunha, “Disruption of Cosmic String Wakes by Gaussian Fluctuations,” *Phys. Rev. D* **93**, no. 12, 123501 (2016) doi:10.1103/PhysRevD.93.123501 [arXiv:1508.02317 [astro-ph.CO]].
- [14] J. Harnois-Deraps, U. L. Pen, I. T. Iliev, H. Merz, J. D. Emberson and V. Desjacques, “High Performance P3M N-body code: CUBEP3M,” *Mon. Not. Roy. Astron. Soc.* **436**, 540 (2013) doi:10.1093/mnras/stt1591 [arXiv:1208.5098 [astro-ph.CO]].
- [15] A. Raccañelli *et al.*, “Measuring redshift-space distortions with future SKA surveys,” arXiv:1501.03821 [astro-ph.CO];
- D. Barbosa, S. Anton, L. Gurwits and D. Maia, “Proceedings, Symposium 7: The Square Kilometre Array: Paving the way for the new 21st century radio astronomy paradigm (JENAM 2010) : Lisbon, Portugal, September 6-10, 2010,” *Astrophys. Space Sci. Proc.*, pp.1 (2012). doi:10.1007/978-3-642-22795-0
- [16] E. Cands, L. Demanet, D. Donoho, and L. Ying, “Fast Discrete Curvelet Transforms,” *Multiscale Model. Simul.*, 5(3), 861899.
- [17] N. Otsu, “A Threshold Selection Method from Gray-Level Histograms,” *IEEE Transactions on Systems, Man, and Cybernetics*, Vol. 9, No. 1, 1979, pp. 62-66.
- [18] R. Bracewell, “Two-Dimensional Imaging” Englewood Cliffs, NJ, Prentice Hall, 1995, pp. 505-537.
- [19] Z. Arzoumanian *et al.* [NANOGrAV Collaboration], arXiv:1801.02617 [astro-ph.HE].
- [20] A. Albrecht and N. Turok, “Evolution Of Cosmic Strings”, *Phys. Rev. Lett.* **54**, 1868 (1985);
- D. P. Bennett and F. R. Bouchet, “Evidence For A Scaling Solution In Cosmic String Evolution”, *Phys. Rev. Lett.* **60**, 257 (1988);
- B. Allen and E. P. S. Shellard, “Cosmic String Evolution: A Numerical Simulation”, *Phys. Rev. Lett.* **64**, 119 (1990);
- C. Ringeval, M. Sakellariadou and F. Bouchet, “Cosmological evolution of cosmic string loops”, *JCAP* **0702**, 023 (2007) [arXiv:astro-ph/0511646];
- V. Vanchurin, K. D. Olum and A. Vilenkin, “Scaling of cosmic string loops”, *Phys. Rev. D* **74**, 063527 (2006) [arXiv:gr-qc/0511159];
- L. Lorenz, C. Ringeval and M. Sakellariadou, “Cosmic string loop distribution on all length scales and at any redshift”, *JCAP* **1010**, 003 (2010) [arXiv:1006.0931 [astro-ph.CO]];
- J. J. Blanco-Pillado, K. D. Olum and B. Shlaer, “Large parallel cosmic string simulations: New results on loop production”, *Phys. Rev. D* **83**, 083514 (2011) [arXiv:1101.5173 [astro-ph.CO]];
- J. J. Blanco-Pillado, K. D. Olum and B. Shlaer, “The number of cosmic string loops”, *Phys. Rev. D* **89**, no. 2, 023512 (2014) [arXiv:1309.6637 [astro-ph.CO]].
- [21] M. Hindmarsh, S. Stuckey and N. Bevis, “Abelian Higgs Cosmic Strings: Small Scale Structure and Loops”, *Phys. Rev. D* **79**, 123504 (2009) doi:10.1103/PhysRevD.79.123504 [arXiv:0812.1929 [hep-th]].
- [22] K. M. Gorski, E. Hivon, A. J. Banday, B. D. Wandelt, F. K. Hansen, M. Reinecke and M. Bartelman, “HEALPix - A Framework for high resolution discretization, and fast analysis of data distributed on the sphere,” *Astrophys. J.* **622**, 759 (2005) doi:10.1086/427976 [astro-ph/0409513].